sustainability

MDPI

Article

Vehicle-Integrated Photovoltaic (VIPV) for Sustainable Airports: A Flexible Framework for Performance Assessment

Hamid Samadi [1], Guido Ala [1,*], Miguel Centeno Brito [2], Giulia Marcon [1], Pietro Romano [1] and Fabio Viola [1]

[1] Department of Engineering, University of Palermo, 90128 Palermo, Italy; hamid.samadi@unipa.it (H.S.); giulia.marcon@unipa.it (G.M.); pietro.romano@unipa.it (P.R.); fabio.viola@unipa.it (F.V.)
[2] Institute of Dom Luiz (IDL), Faculty of Sciences, University of Lisbon, 1749-016 Lisbon, Portugal; mcbrito@ciencias.ulisboa.pt
* Correspondence: guido.ala@unipa.it

Abstract

Airports are among the most energy-intensive infrastructures, and the decarbonization of ground operations is essential to achieving sustainable aviation goals. Vehicle-integrated photovoltaic (VIPV) offers a promising strategy to complement electrification by enabling on-board renewable generation. While previous studies have mainly focused on fixed PV installations such as rooftops or carports, the potential of VIPV in airports has largely been overlooked, and no structured methodology has been established to investigate it. This study addresses this gap by proposing a two-scenario framework for assessing VIPV performance. The first scenario, named the Generalized Approach, estimates annual energy production based on irradiance data, vehicle surface area, and driving-to-standby ratios. The second scenario, named the Data-Driven Approach, incorporates detailed GPS-based driving data to capture the dynamic effects of orientation, speed, and operating conditions. Applied to European and Middle Eastern airports, the framework showed that VIPV could cover 1700–5500 km/year for buses, 650–5000 km/year for minibuses, and 840–6180 km/year for luggage tractors, with avoided emissions strongly influenced by local grid intensity. Grid parity analysis indicated favorable conditions in sunny, high-cost electricity markets. The framework is transferable to other VIPV applications and provides a practical tool for evaluating their technical, environmental, and economic potential.

Keywords: vehicle-integrated photovoltaic (VIPV); airport ground vehicles; solar vehicles in airport

check for updates

Academic Editor: Alireza Dehghani-Sanij

Received: 19 September 2025
Revised: 13 October 2025
Accepted: 15 October 2025
Published: 17 October 2025

Citation: Samadi, H.; Ala, G.; Brito, M.C.; Marcon, G.; Romano, P.; Viola, F. Vehicle-Integrated Photovoltaic (VIPV) for Sustainable Airports: A Flexible Framework for Performance Assessment. *Sustainability* **2025**, *17*, 9246. https://doi.org/10.3390/su17209246

Copyright: © 2025 by the authors. Licensee MDPI, Basel, Switzerland. This article is an open access article distributed under the terms and conditions of the Creative Commons Attribution (CC BY) license (https://creativecommons.org/licenses/by/4.0/).

1. Introduction

The global transition toward low-carbon mobility is accelerating, with growing emphasis on reducing greenhouse gas emissions across all transport sectors. Airports, as complex and energy-intensive infrastructures, are central to this transformation [1]. While much of the attention has focused on aircraft emissions, ground operations also account for a significant share of the environmental footprint. Decarbonizing these activities has therefore become a priority, with electrification of ground support vehicles (GSVs), including baggage tractors and buses, emerging as a key step toward sustainable airport operations [2,3].

Electrification, however, increases dependence on charging infrastructure and grid electricity, which may still be partially supplied from fossil-based sources [4,5]. Integrating

renewable energy directly into vehicles through vehicle-integrated photovoltaic (VIPV) offers a complementary solution. By generating electricity at the point of use, VIPV can reduce charging needs, improve operational flexibility, and contribute to emission reduction targets [6,7]. Despite these advantages, the application of VIPV in airports has received very limited attention. Most existing research and real-world deployments of PV in airports remain focused on fixed installations such as rooftops, carports, or ground-mounted systems [8,9].

The technical evaluation of VIPV poses its own challenges, as the energy yield depends not only on solar resources and installed PV surface but also on vehicle movement, orientation, and operational cycles. In practice, VIPV evaluation is complicated by constantly changing boundary conditions, including dynamic exposure to sunlight, motion-induced shading, and aerodynamic constraints on PV placement [10]. Experimental investigations have contributed to understanding these factors, for instance by monitoring irradiance on PV-equipped vehicles under real driving conditions. Such studies consistently confirm that the roof surface receives the most radiation, but that lateral and rear panels experience strong variability depending on route geometry and solar angle [11–13]. However, experimental testing remains costly, site-specific, and difficult to generalize, making it less practical for early-stage analysis.

Numerical simulations can reproduce irradiance dynamics, shading, and temperature variations under different environmental conditions, offering valuable insights before physical prototypes are built [14]. For example, hourly models have been applied to estimate annual solar yields for commercial vans and trucks in Europe [15] and to assess the potential of integrating PV modules on the roofs of emergency vehicles during disasters in Italy [16], whereas higher time-resolution approaches, such as one-minute simulations, have been developed for trains and buses to capture the influence of local shading and surrounding geometry [17,18]. Other works have coupled electrical and thermal sub-models, typically using the single-diode equation to reproduce current–voltage characteristics and temperature models like NOCT (Nominal Operating Cell Temperature) to describe thermal effects [19,20]. Together, these studies demonstrate the diversity of existing approaches but also reveal the absence of a unified framework that connects and supports both simplified and detailed analyses.

The present study tries to address this gap by introducing a comprehensive modeling framework that integrates multiple simulation levels within a consistent structure. The proposed methodology combines a generalized, low-data scenario with a data-driven configuration capable of incorporating real vehicle motion. In the first scenario, hourly irradiance data and representative efficiency parameters are used to estimate long-term energy production on the vehicle roof and result in avoided emissions and grid parity. In the second scenario, the temporal resolution increases to one-second intervals, with GPS-based measurements of vehicle position, azimuth, and speed used to compute instantaneous irradiance on multiple vehicle surfaces. The Faiman temperature model [21] is applied to capture the effects of ambient temperature and wind speed, which are particularly relevant in airport environments characterized by open exposure and variable airflows. This combination allows for a smooth transition from broad feasibility screening to detailed operational analysis, bridging the gap between simplified and data-intensive modeling approaches.

The first scenario offers a generalized approach that does not rely on detailed driving behavior. Vehicle (bus, luggage truck, etc.) activity is simplified into driving and standby modes, represented by time fractions for each hour. This allows for the use of global horizontal irradiance applied to the vehicle roof, combined with simplified assumptions such as flat road conditions, general losses, and performance ratios. While simple, this

scenario enables long-term assessments of technical, economic, and environmental potential using readily available data, making it particularly valuable as an accessible entry point for early-stage analyses (particularly in airport applications).

The second scenario, by contrast, is designed for applications where detailed driving data are available. Vehicle position, orientation, and speed are incorporated to calculate dynamic irradiance on multiple surfaces, allowing for a more accurate representation of real-world operating conditions. This scenario can accommodate both repetitive driving cycles and variable operational profiles, enabling deeper investigation of VIPV performance, operational strategies, and system-level impacts.

The novelty of this study lies in two key aspects. First, it organizes the methodology into a coherent and transferable framework, filling the gap between oversimplified models and data-intensive approaches. Second, it applies this framework to the underexplored case of airport ground vehicles, thereby highlighting a promising application domain for VIPV. While the airport case study demonstrates the potential of the methodology, the framework is designed to be flexible and transferable, offering a structured reference for assessing VIPV in a wide range of transport sectors.

Through this contribution, the study provides both a methodological foundation and a practical demonstration of VIPV's potential, supporting researchers, engineers, and decision-makers in advancing sustainable mobility. By integrating renewable generation directly into vehicle fleets, the proposed framework may contribute to the broader goal of achieving zero-emission and energy self-sufficient airport operations.

2. Methodology

2.1. General PV Power Model

The power output of a PV system can be expressed as [16]:

$$P = \eta \cdot G \cdot A_{PV} \tag{1}$$

where η is the overall system efficiency, G is the incident solar irradiance (W/m^2), and A_{PV} is the effective PV area (m^2). The overall efficiency is defined as the product of the PV module efficiency (η_{PV}) and the efficiency of the power conversion system (η_{Conv}).

$$P = \eta_{PV} \cdot \eta_{Conv} \cdot G \cdot (A_{Sur} \cdot \alpha) \tag{2}$$

Here A_{Sur} is the available geometric surface area of the vehicle, and α is the coverage ratio that accounts for the fraction of usable surface suitable for PV installation. Solar irradiance (G) is composed of three main components: direct (beam), diffuse, and reflected [22].

$$G = G_b + G_d + G_r \tag{3}$$

In this study, only the direct and diffuse components were considered. To better approximate real operating conditions, two correction factors were introduced:

- A curvature factor ($CF = 0.9$) to account for reduced effective capture due to curved vehicle surfaces [23];
- A shading loss factor ($\eta_{Shading} = 0.75$) representing partial obstruction from nearby objects or the vehicle itself.

Thus, the effective irradiance was calculated as:

$$G = [(\eta_{\ Shading} \cdot G_b) + G_d] \cdot CF \tag{4}$$

2.2. Scenario 1: Generalized Approach

In the first scenario, vehicle operation was simplified into two modes: driving and standby. This approach is particularly relevant when detailed driving data are not available. The fraction of time spent in each mode was represented by a driving-to-standby ratio (R), applied on an hourly basis.

Energy generation in each mode was estimated as [15,16]:

$$E_{Driving} = \sum_{n=1}^{8760} \eta_{PV} \cdot \eta_{Conv} \cdot G_h \cdot (A_{Sur} \cdot \alpha) \cdot PR \cdot R \quad (5)$$

$$E_{Standby} = \sum_{n=1}^{8760} \eta_{PV} \cdot \eta_{Conv} \cdot G_h \cdot (A_{Sur} \cdot \alpha) \cdot PR \cdot (1 - R) - L \quad (6)$$

$$E = E_{Standby} + E_{Driving} \quad (7)$$

where L represents standby charging losses (W), G_h represents hourly irradiance (W/m^2), PR represents the performance ratio, and R represents the driving-to-park ratio. The performance ratio was calculated as [16]:

$$PR = \frac{PV_{OUT}}{\frac{GTI_{opta}}{H_{STC}}} \quad (8)$$

where PV_{OUT} is specific photovoltaic power output (kWh/kW$_P$ per Year) and GTI_{opta} is the global tilted irradiance at the optimum angle (kWh/m^{2}per Year). These parameters for each region are available on the Global Solar Atlas [24]. It should also be noted that the standard test condition irradiance (H_{STC}) is taken as 1000 (W/m^2), which is the internationally recognized reference solar irradiance level used for evaluating PV system performance under ideal conditions.

This scenario provided long-term estimates of annual energy yield under simplified assumptions, enabling further evaluation of sustainability and economic performance.

2.3. Scenario 2: Data-Driven Approach

When detailed driving data were available, a more comprehensive scenario was applied. This approach accounted for additional effects such as thermal behavior, vehicle speed, and irradiance on multiple surfaces (roof, sides, and rear).

The temperature-corrected power output is expressed as [18,20]:

$$P = \eta_{PV} \cdot \eta_{Conv} \cdot G \cdot (A_{Sur} \cdot \alpha) \cdot \left(1 + k \cdot \left(T - T_{ref}\right)\right) \quad (9)$$

The PV module temperature (T) was estimated using the Faiman model [21,25]:

$$T = T_a + \frac{G}{U_0 + U_1 \cdot WS} \quad (10)$$

$$WS_{Roof} = WS_{TMY} \cdot \left(\frac{h_{Roof}}{10^{0.2}}\right) \quad (11)$$

where T_a represents the air temperature, U_0 represents the constant heat transfer component W/m^{2}K, U$_1$ represents the convective heat transfer component W/m^{3}sK, and WS represents the wind speed m/s. Since wind speed data from Typical Meteorological Year (TMY) files are given at 10 m height, they were adjusted to the height of the vehicle roof, using Equation (13). It should be noted that, when the vehicle is stopped (Speed = 0), the wind speed is adjusted based on the height of the minibus roof to simulate natural airflow.

When the vehicle is in motion, the wind speed is considered the same as the vehicle speed, thus neglecting the wind speed.

For irradiance estimation, the model extended calculations beyond the roof to all relevant vehicle surfaces. The direct and diffuse irradiance on a tilted surface were calculated as [22,26,27]:

$$G_b = DNI \cdot [cos(\beta) \cdot cos(\theta_Z) + sin(\beta) \cdot sin(\theta_Z) \cdot cos(\gamma_S - \gamma)] \quad (12)$$

$$G_d = DHI \cdot \left[\frac{(1 - F_1) \cdot (1 + cos\beta)}{2} + F_1 \cdot \frac{A}{B} + F_2 \cdot sin\beta \right] \quad (13)$$
$$A = \max(0, cosAOI), \quad B = \max(0.087, cos\theta_Z)$$

where DNI and DHI are the direct normal and diffuse horizontal irradiance, respectively; β is the surface tilt angle; θ_Z is the solar zenith angle; γ_S is the solar azimuth angle; and γ is the surface azimuth. The coefficients F_1 and F_2 are circumsolar and horizon brightening factors, respectively, which adjust the distribution of diffuse irradiance.

These equations, originally developed for fixed PV systems, were adapted to moving vehicles by discretizing the driving pathway into one-second intervals. At each step, the sun's position relative to each vehicle surface was calculated using driving data (latitude, longitude, orientation, and speed). The modelling was implemented using VIPVLIB [28], an extended version of PVLIB [29] developed to capture vehicle dynamics and VIPV-specific conditions.

2.4. Environmental and Economic Assessment

Beyond energy yield, two additional performance metrics were evaluated.

- Avoided emissions (Em_{Avoid}) were calculated as [16]:

$$Em_{Avoid} = E \cdot CI \quad (14)$$

where E represents the annual energy production (kWh) and CI is the carbon intensity of the regional grid ($kgCO_2/kWh$). Since carbon intensity varies significantly between regions, being higher in grids dominated by fossil fuels and lower in those with larger shares of renewables, the environmental benefits of deployment are strongly location-dependent.

- Levelized Cost of Electricity (LCOE) was used to evaluate economic feasibility [30]

$$LCOE = \frac{C_{life}}{E_{life}} \quad (15)$$

where E_{life} represents the total lifetime energy production, and C_{life} represents the total life cycle cost. This metric provides the average cost of electricity generation over the system lifetime, enabling direct comparison of VIPV with grid electricity and other energy technologies.

3. Case Studies

To demonstrate the applicability of the proposed framework, two sets of case studies were conducted, corresponding to the two scenarios defined in the methodology. Scenario 1 emphasizes a generalized assessment across multiple geographical locations, while Scenario 2 focuses on detailed route-based analyses using real driving data.

3.1. Scenario 1

In the first scenario, simulations were carried out for a range of international airports to investigate the influence of climatic conditions, grid carbon intensity, and electricity

prices on VIPV performance. Three Italian cities, Milan, Rome, and Palermo, were selected to represent different climatic regions and electricity price levels within a common national framework, while also reflecting differences in airport scale and operational characteristics. To extend the analysis within Europe, three additional airports in Lisbon, Frankfurt, and Copenhagen were considered, capturing diverse solar resources and market conditions. Finally, three major hub airports in Doha, Dubai, and Istanbul were included to highlight environments with high solar potential and global strategic importance, despite their comparatively lower electricity prices.

Figure 1 presents the carbon intensity of national electricity grids in 2024 [31], together with non-household electricity prices. Among the European cities, Lisbon exhibited the lowest emissions factor (0.101 kg CO_2 per kWh), while Doha showed the highest (0.49 kg CO_2 per kWh), reflecting the heavy reliance on fossil fuels in its energy mix. Electricity prices displayed a wide variation, from €0.03 per kWh in Doha to €0.27 per kWh in Copenhagen, providing an important benchmark for assessing grid parity [32–34].

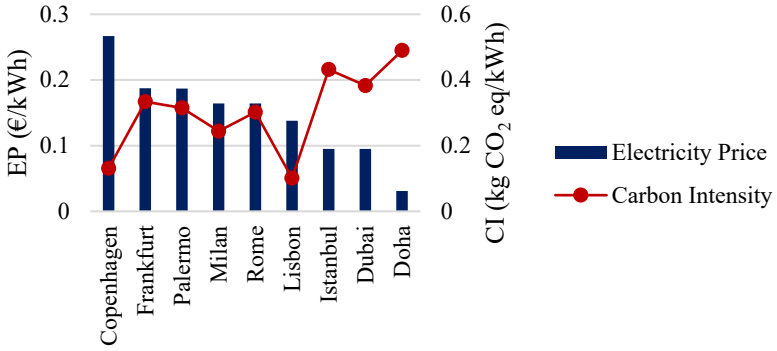

Figure 1. Non-household electricity price and carbon intensity across different cities [31–34].

For all locations, the PV system lifetime was assumed to be 10 years with an annual degradation rate of 1%. Although fixed PV installations often achieve lower degradation values, the conservative assumption reflects the more demanding operating conditions of VIPV systems, including vibration, intermittent shading, thermal cycling, and mechanical wear. The PV module efficiency was assumed to be approximately 21%, corresponding to a power density of 210 W_p/m^2, which was used to calculate the available installed capacity [15].

3.2. Scenario 2

Unlike vehicles that follow fixed or repetitive drive cycles, airport ground vehicles operate along highly variable and often unpredictable routes. Their movement depends on daily operational needs, which means trips rarely follow a standardized pattern. This makes it challenging to define representative duty cycles for simulation. Therefore, Scenario 2 was designed not to establish general driving cycles but to show the capability of the proposed framework to integrate real-world driving data and capture the dynamic effects of vehicle motion on VIPV performance.

The analysed datasets correspond to passenger shuttle buses operating at normal commercial airports, transferring passengers between aircraft and terminals. Because these data were based on real operating conditions, they inherently reflect many contextual factors such as airport size, apron configuration, trip type (arrival, departure, or towing), and local congestion. As a result, each dataset provides a realistic snapshot of typical movement patterns within airport environments.

To illustrate this approach, GPS-based datasets from four international airports were analysed: Istanbul Sabiha Gökçen, Rome Fiumicino, Milan Bergamo, and Palermo Airport. Figure 2 shows the routes of the vehicles during several trips at these airports.

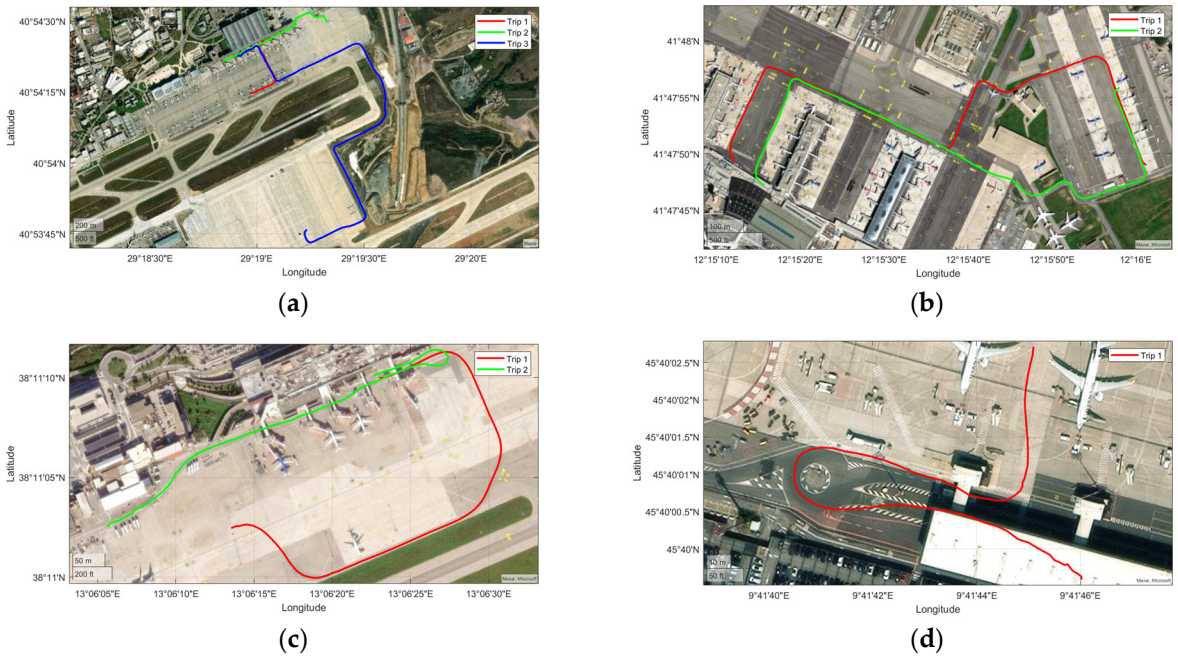

Figure 2. The vehicle routes during representative trips at four airports: (**a**) Istanbul Sabiha Gökçen, (**b**) Rome Fiumicino, (**c**) Palermo, and (**d**) Milan Bergamo (Source: MATLAB R2023b).

At Istanbul Sabiha Gökçen Airport, three independent trips were available, ranging in duration from 3 to 10 min. The variety in trip length, route geometry, and vehicle orientation offered valuable insight into the influence of operational diversity on VIPV performance. At Rome Fiumicino and Palermo airports, two trips were analysed in each case, lasting approximately 5 min and 2 min, respectively. Finally, a single 1-min trip was considered at Milan Bergamo Airport. Figure 3 presents the corresponding speed and azimuth profiles, highlighting the variability across the datasets.

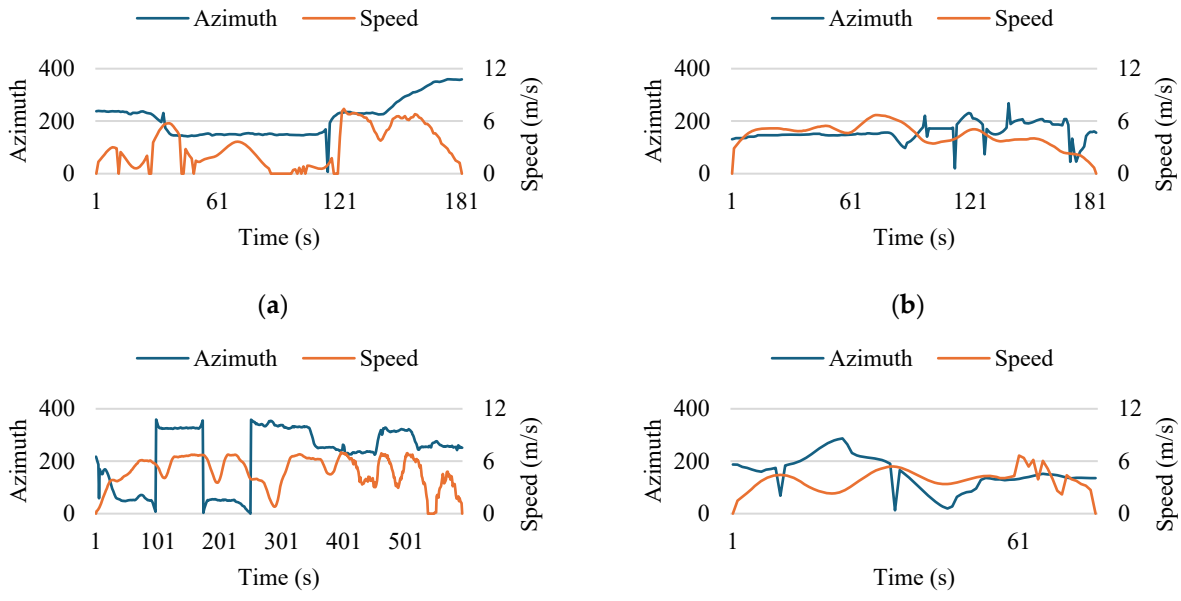

Figure 3. *Cont.*

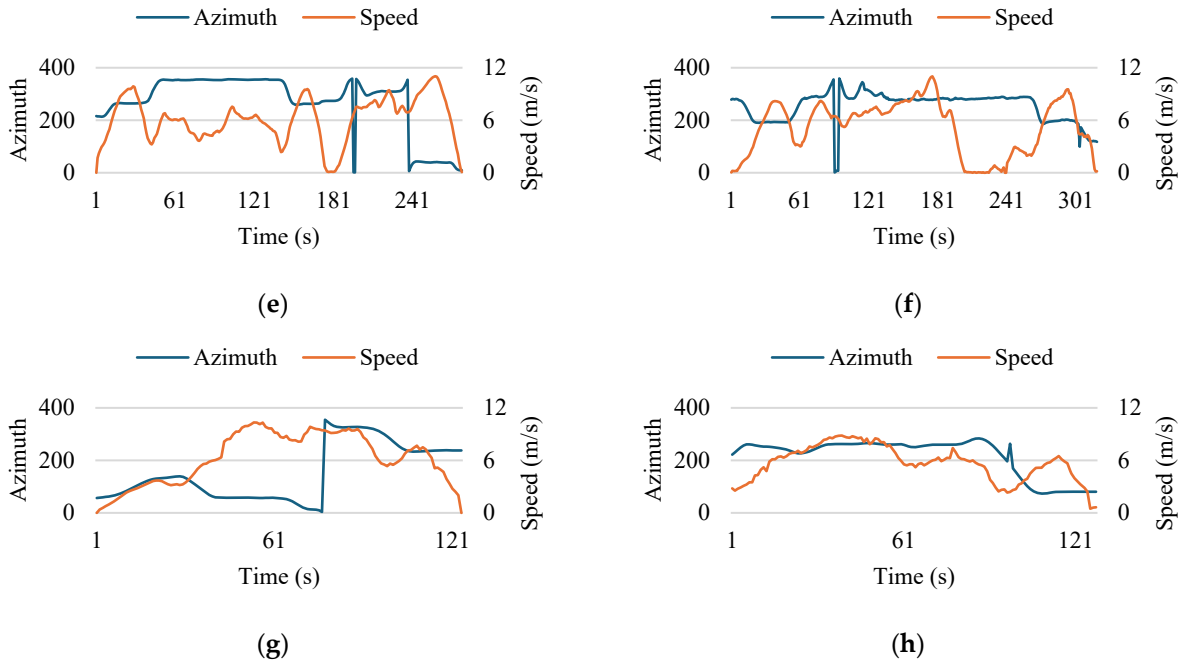

Figure 3. Vehicle speed profiles and azimuth angle variations during trips: Istanbul (**a**) Trip 1, (**b**) Trip 2, (**c**) Trip 3; Milan (**d**); Rome (**e**) Trip 1, (**f**) Trip 2; Palermo (**g**) Trip 1, (**h**) Trip 2.

While the duration of some trips, such as the one at Milan Bergamo Airport, is short, these real datasets effectively demonstrate how the framework performs under diverse and realistic operational conditions. The variability among airports, routes, and time spans provides a useful cross-section of airport operations. Longer datasets would indeed enable seasonal or probabilistic analysis, but even with limited samples, the framework can identify trends and sensitivities related to solar exposure, orientation, and movement dynamics.

To improve robustness, future studies could expand the dataset and include confidence intervals to quantify the variability across different trip categories (arrivals vs. departures) or congestion levels. Nevertheless, in the author's opinion, the current results already demonstrate the flexibility of the framework and its applicability to operational data typical of passenger airports.

It should be noted that the values of efficiency of the power converter (η_{Co}) and reference temperature (T_{ref}) were set to 96% and 25 °C, respectively [18]. The PV module technology used in the simulations was crystalline silicon (c-Si). Detailed electrical and thermal parameters of the module technology are provided in Table 1.

Table 1. Specifications and electrical parameters of the crystalline silicon PV modules used in the simulations [35].

PV Module	Efficiency [%]	k [%/°C]	U_0 [W/m^2°C]	U_1 [W/m^3°C]
c-Si	21.6	−0.47	30.02	6.28

4. Results

4.1. Scenario 1

To investigate the technical feasibility of VIPV under different operating conditions, a sensitivity analysis was carried out on two key parameters: standby charging losses (L) and the driving-to-park ratio (R). Since the first scenario is generalized and considers the vehicle in driving or parked mode within each hour, different values of these parameters can represent a wide range of real operating conditions, reflecting how often the vehicle

is in motion and how much energy is consumed by auxiliary systems when stationary. This approach allows for the evaluation of system behavior without requiring detailed trip data, while still capturing the main effects of usage patterns and standby consumption on overall performance.

Standby losses represent the auxiliary consumption required to keep systems active while the vehicle is parked (e.g., BMS operation, etc.). Two levels were considered: 100 W (L1, low-loss) and 700 W (L2, high-loss) [16]. The driving-to-park ratio ranged across four values: 0.2 (R1), 0.4 (R2), 0.6 (R3), and 0.8 (R4), to simulate different operational profiles ranging from predominantly parked to highly active use.

Annual energy production was first estimated across nine cities, for installed PV areas ranging from 3 to 30 m^2. Figure 4 illustrates representative results for selected cases (R1L1, R1L2, R3L1, and R3L2). These combinations were selected to show the influence of both operational factors, the proportion of driving time (R) and the magnitude of standby losses (L), on the yearly energy balance. Comparing R1 and R3 highlights the impact of more intensive vehicle use, while comparing L1 and L2 reveals how auxiliary consumption can reduce the net energy gain, particularly for systems with limited installed area.

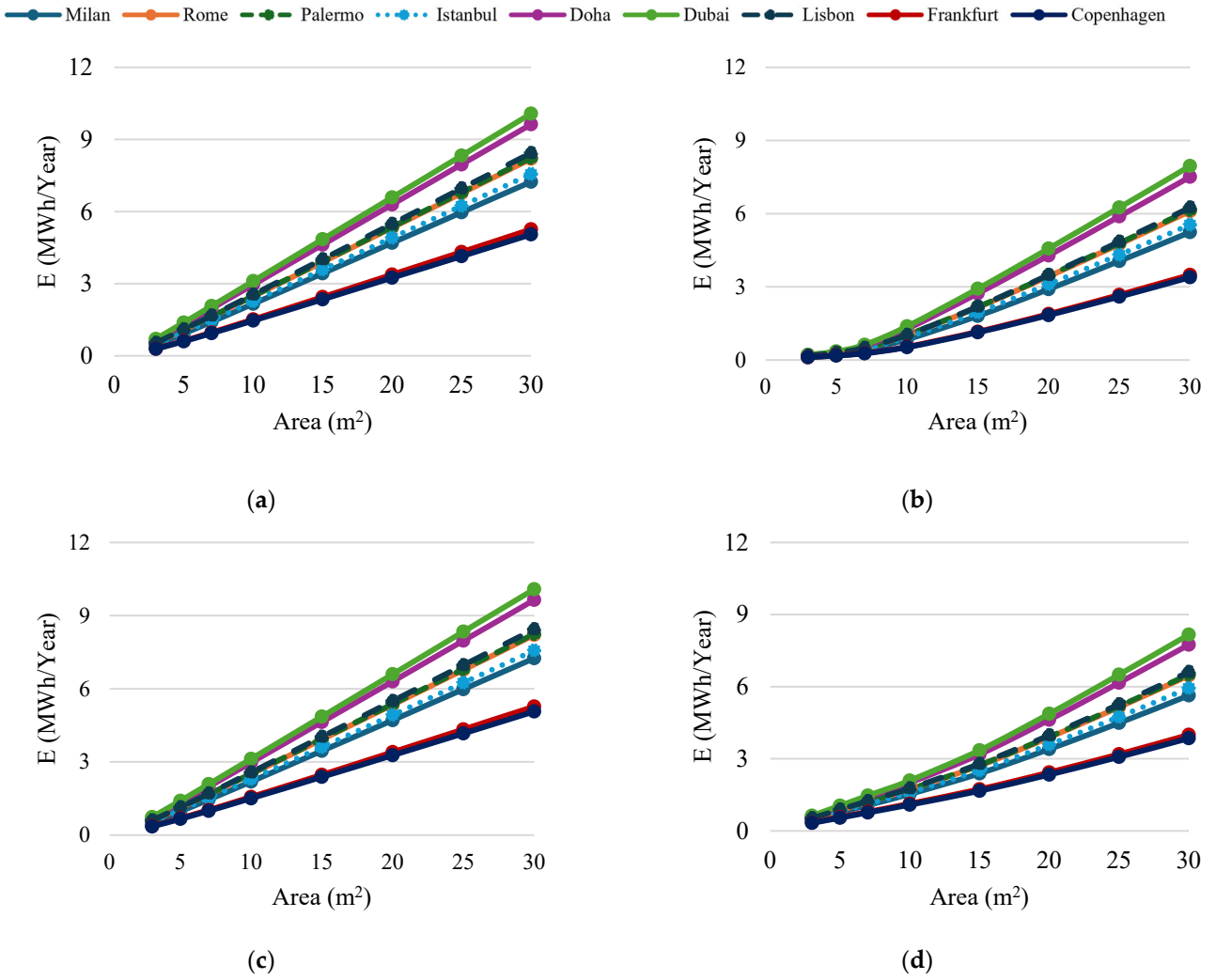

Figure 4. Yearly energy production of VIPV systems for different cities and PV areas under selected operating conditions: (**a**) R1L1, (**b**) R1L2, (**c**) R3L1, (**d**) R3L2.

Under low-loss conditions (L1), energy generation increases almost linearly with PV area. However, under high-loss conditions (L2), the increase becomes nonlinear, especially for small PV areas where standby consumption represents a large fraction of the total power harvested. Across all cases, Doha and Dubai produced the highest annual yields due to their high solar resource, followed by Palermo, Rome, and Lisbon, while Copenhagen and Frankfurt showed the lowest performance.

Another analysis focused on three representative PV areas: 3 m^2 (luggage tractor), 7 m^2 (minibus), and 20 m^2 (bus). For each class of vehicle, the achievable solar driving range was calculated by dividing the annual energy yield by the average consumption per kilometer. Results (Figure 5) showed ranges of:

- Buses (1.2 kWh/km) [20]: ~1700–5500 km/year,
- Minibuses (0.47 kWh/km) [36]: ~650–5000 km/year,
- Luggage trucks (0.13 kWh/km) [37]: ~840–6180 km/year.

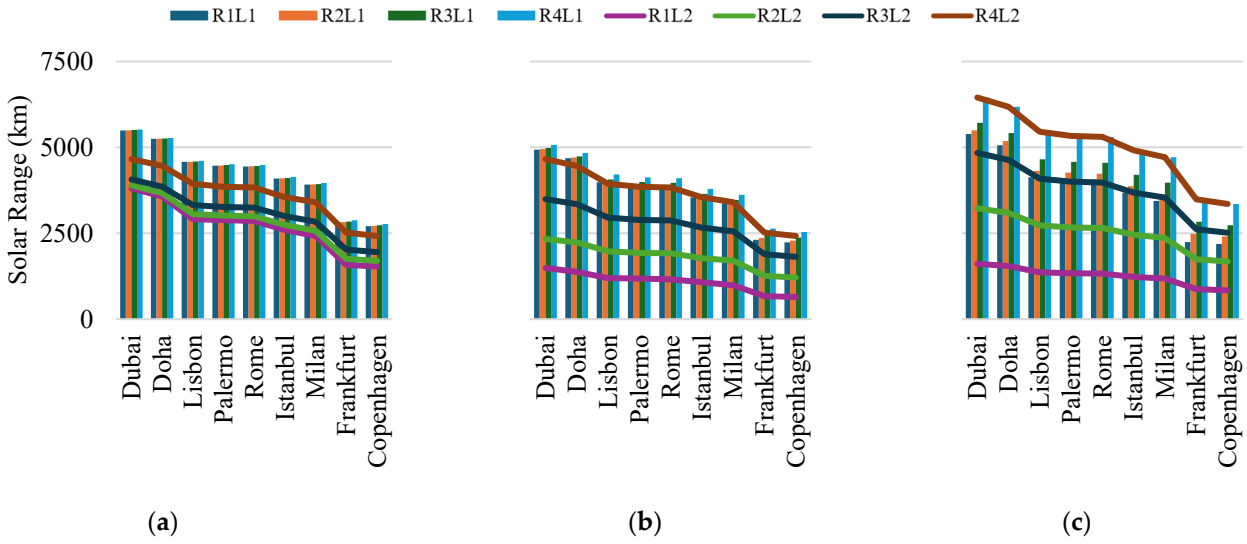

Figure 5. Yearly solar driving range achievable by VIPV for three representative vehicle types: (**a**) bus (20 m^2 PV), (**b**) minibus (7 m^2 PV), and (**c**) luggage tractor (3 m^2 PV), under different cities and working conditions.

These findings demonstrate that even under conservative assumptions, VIPV could cover a meaningful portion of yearly driving needs, particularly in sunny locations. In addition, Figure 6 presents the variations in daily energy production obtained from the VIPV system for the minibus (7 m^2 PV) across different cities within the R3L2 driving profile. This example was selected to illustrate how local climatic conditions and seasonal irradiance significantly influence the achievable energy yield.

Environmental benefits were quantified as avoided CO_2 emissions by multiplying annual generation by the regional grid carbon intensity. Figure 7 shows that avoided emissions strongly depend not only on irradiance but also on the carbon intensity of the local grid. For example, Lisbon, with relatively low grid carbon intensity, yielded modest avoided emissions despite good irradiance, whereas Doha and Dubai, with highly carbon-intensive grids, exhibited the largest potential reductions.

To provide a broader context, these results can be related to the macro-scale CO_2 emissions of the transport sector, which account for nearly 30% of total energy-related greenhouse gas emissions in the European Union [38]. Although the absolute contribution of a single VIPV-equipped vehicle is modest, the cumulative impact across large public or commercial fleets could be significant. Therefore, while the results in Figure 7 mainly

illustrate the influence of local solar resource and grid mix, they also highlight the potential of VIPV systems to contribute to the decarbonization of the transport sector.

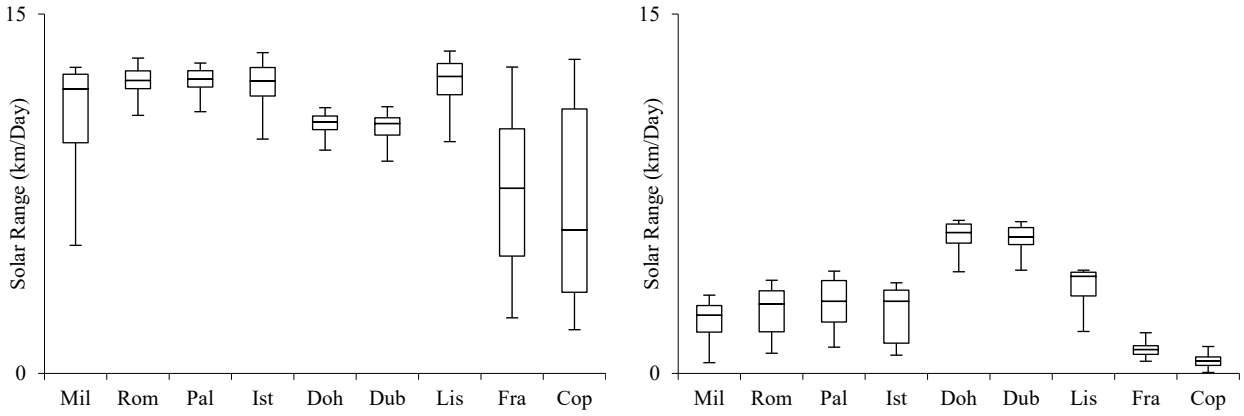

Figure 6. Daily solar driving range achievable by VIPV for the minibus (7 m^2 PV) in R3L2: (**a**) July (**b**) December.

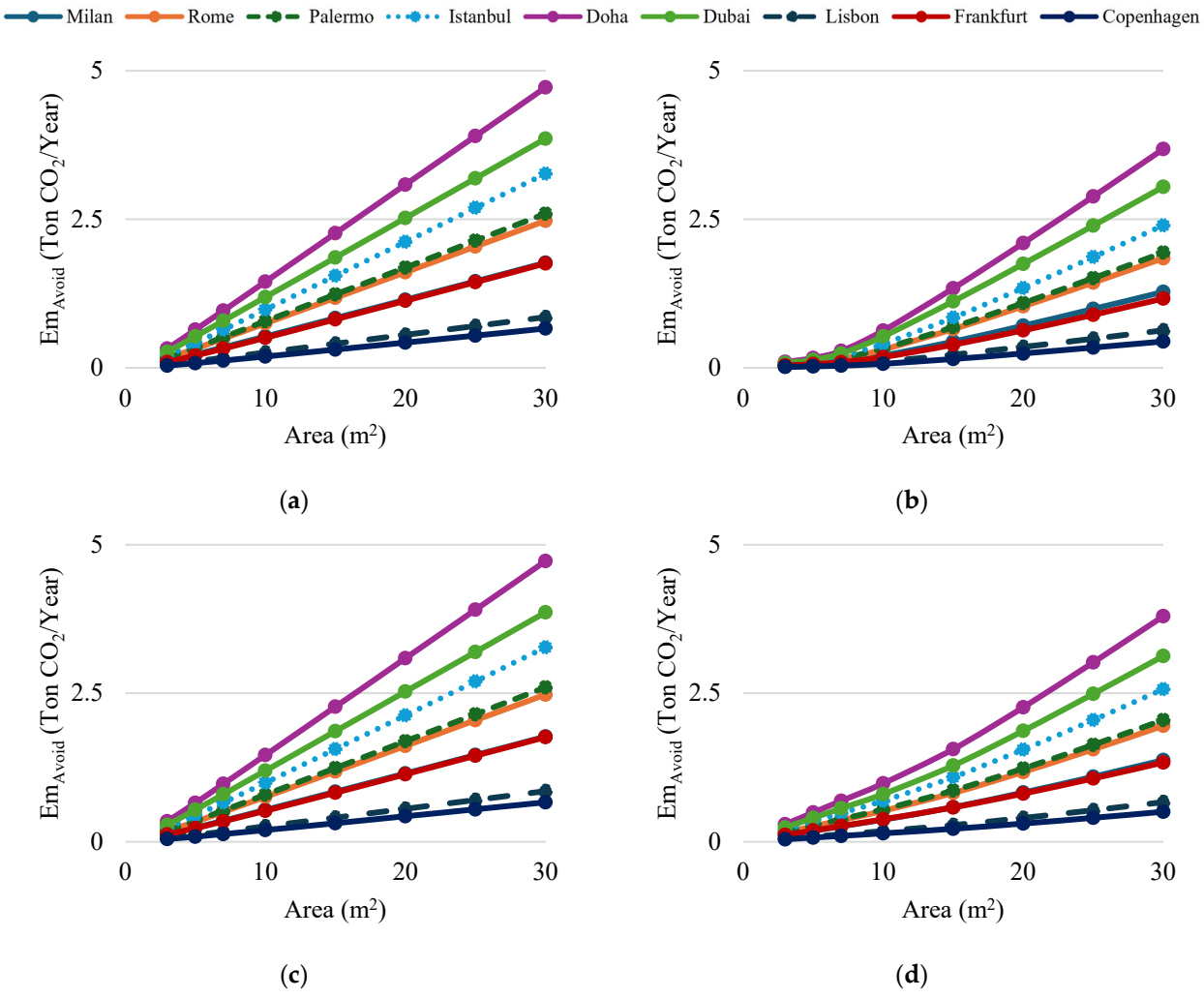

Figure 7. Yearly avoided CO_2 emissions from VIPV systems in different cities and PV areas under selected operating conditions: (**a**) R1L1, (**b**) R1L2, (**c**) R3L1, (**d**) R3L2.

Finally, the economic potential of VIPV was analysed using the Levelized Cost of Electricity (LCOE) as a benchmark for grid parity. Under operating conditions R3L1 (moderate driving, low losses) and R3L2 (moderate driving, high losses), results were compared against regional electricity prices assuming a $WACC_{real}$ of 3% (Figure 8). Additional sensitivity analyses at $WACC_{real}$ values of 2% and 5% were performed for the R3L2 case (Figure 9).

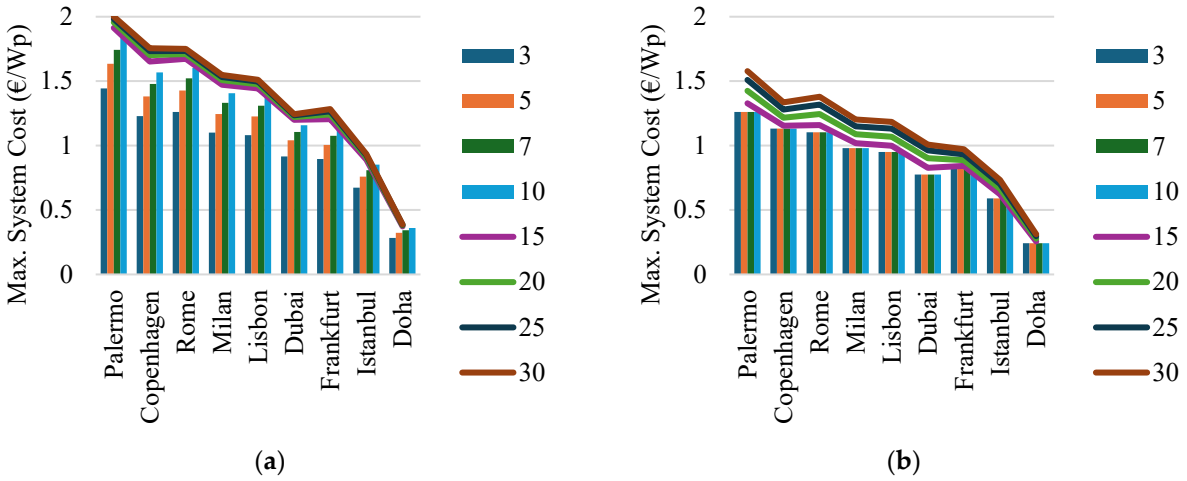

Figure 8. Maximum system costs at grid parity for different cities under $WACC_{real}$ = 3%: (**a**) R3L1, (**b**) R3L2.

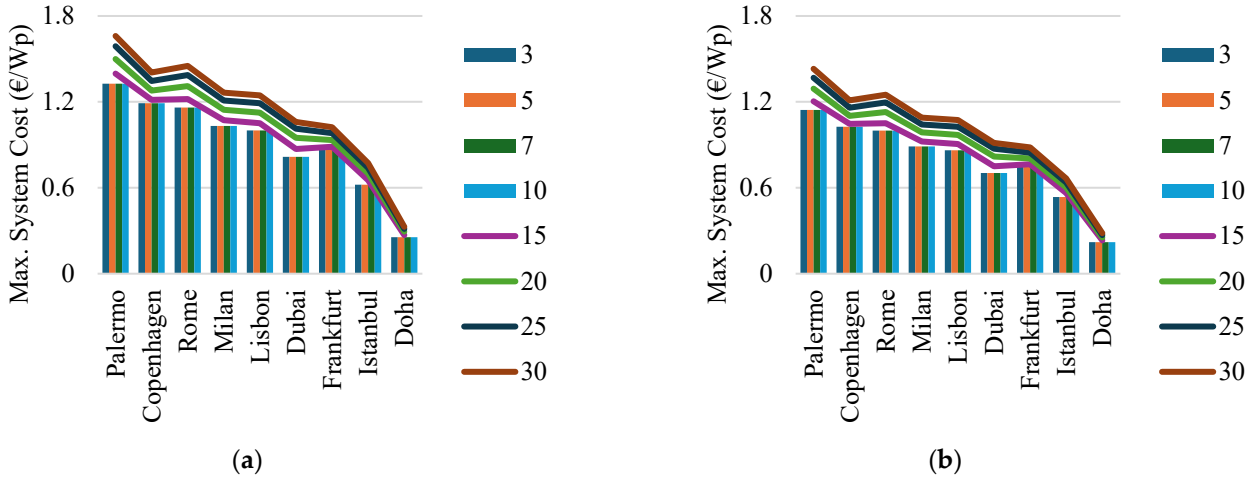

Figure 9. Maximum system costs at grid parity for different cities under operating condition R3L2 with: (**a**) $WACC_{real}$ = 2%, (**b**) $WACC_{real}$ = 5%.

4.2. Scenario 2

Figure 10 shows PV module temperature profiles for trips in Istanbul, Rome, Milan, and Palermo. The influence of both ambient conditions and vehicle speed on module temperature is evident, with higher irradiance and lower airflow leading to higher module temperatures.

Figures 11 and 12 illustrate the energy production per square meter of PV integrated into different vehicle surfaces (roof, sides, rear) for trips conducted at different times of the day (morning vs. afternoon) and seasons (30 July vs. 27 December). In this analysis, the same driving paths were simulated under different time and seasonal conditions to assess how solar energy harvesting varied. By keeping the route geometry and speed profiles constant while varying the day and hour of operation, it was possible to isolate the

influence of seasonal irradiance and diurnal angles of incidence on the energy yield of each surface. As expected, July trips produced higher energy due to greater solar elevation and irradiance, whereas December trips exhibited lower production and stronger asymmetry between surfaces.

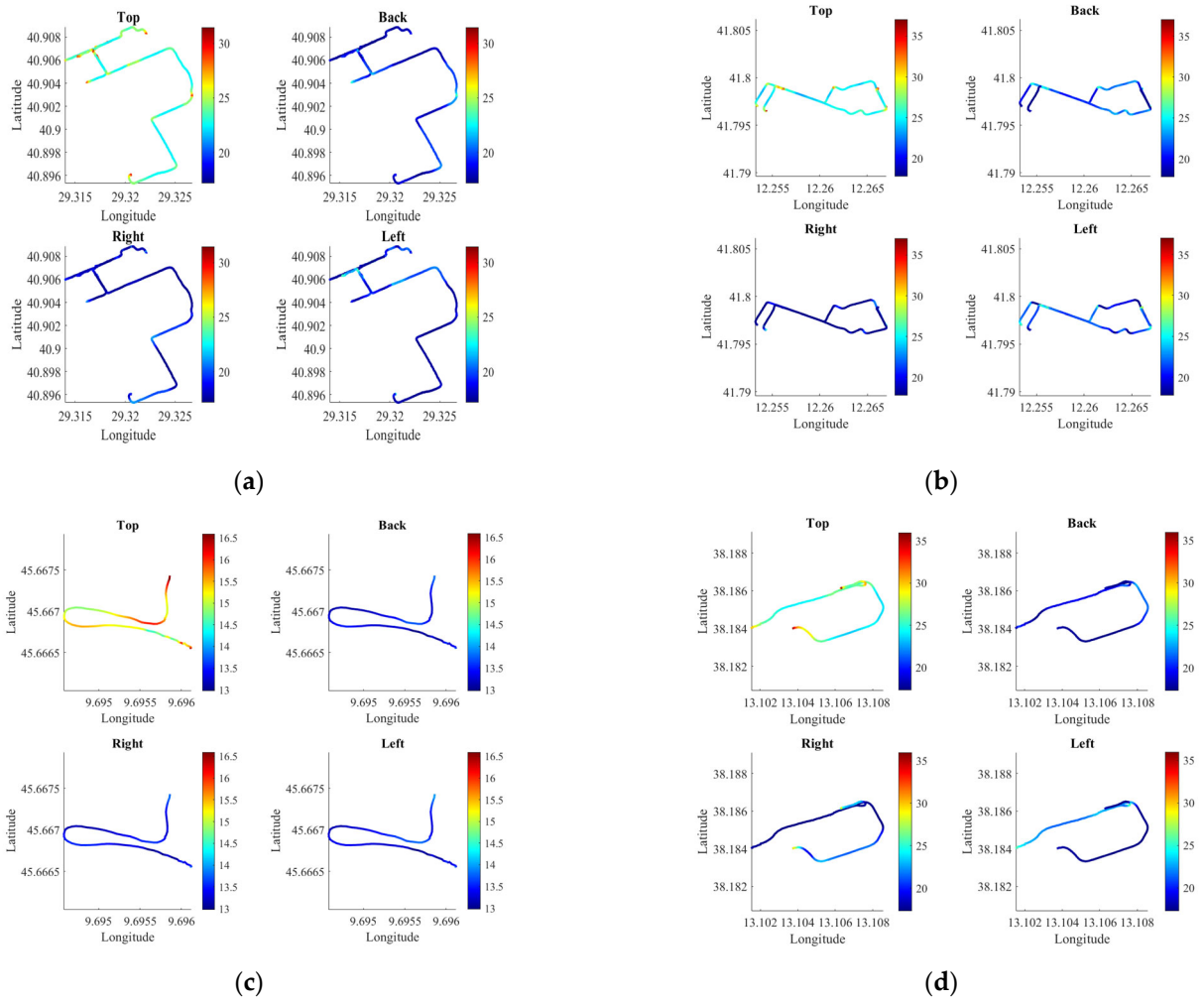

Figure 10. Temperature variations in PV modules integrated on vehicle surfaces during trips at: (**a**) Istanbul, (**b**) Rome, (**c**) Milan, and (**d**) Palermo.

These figures highlight the variations in energy generation results between different trips, which are primarily influenced by the changing azimuth angles of each vehicle surface throughout the journeys. Because the orientation of the vehicle relative to the sun varies with the path taken, each surface (top, back, left, and right) experiences different irradiance levels depending on its alignment during the trip. This effect becomes more pronounced when trips occur at different times of the day, due to the sun's movement, and during different seasons, as demonstrated by the simulations on 30 July and 27 December.

The trip analysed in Milan was relatively short at less than two minutes. This reflects a common scenario in certain airports where the distance between aircraft and terminals is minimal, and as a result, shuttle buses may not be used extensively and often remain parked. This situation presents an opportunity: when vehicles are not in use, they can be parked in non-shaded areas, fully exposed to sunlight to maximize solar energy harvesting. Furthermore, since the vehicle's energy consumption is zero during these times, the generated solar energy can be stored for later use. Consequently, this stored energy can

contribute to vehicle operation during active periods, effectively increasing the solar range and improving the overall utility of the VIPV system.

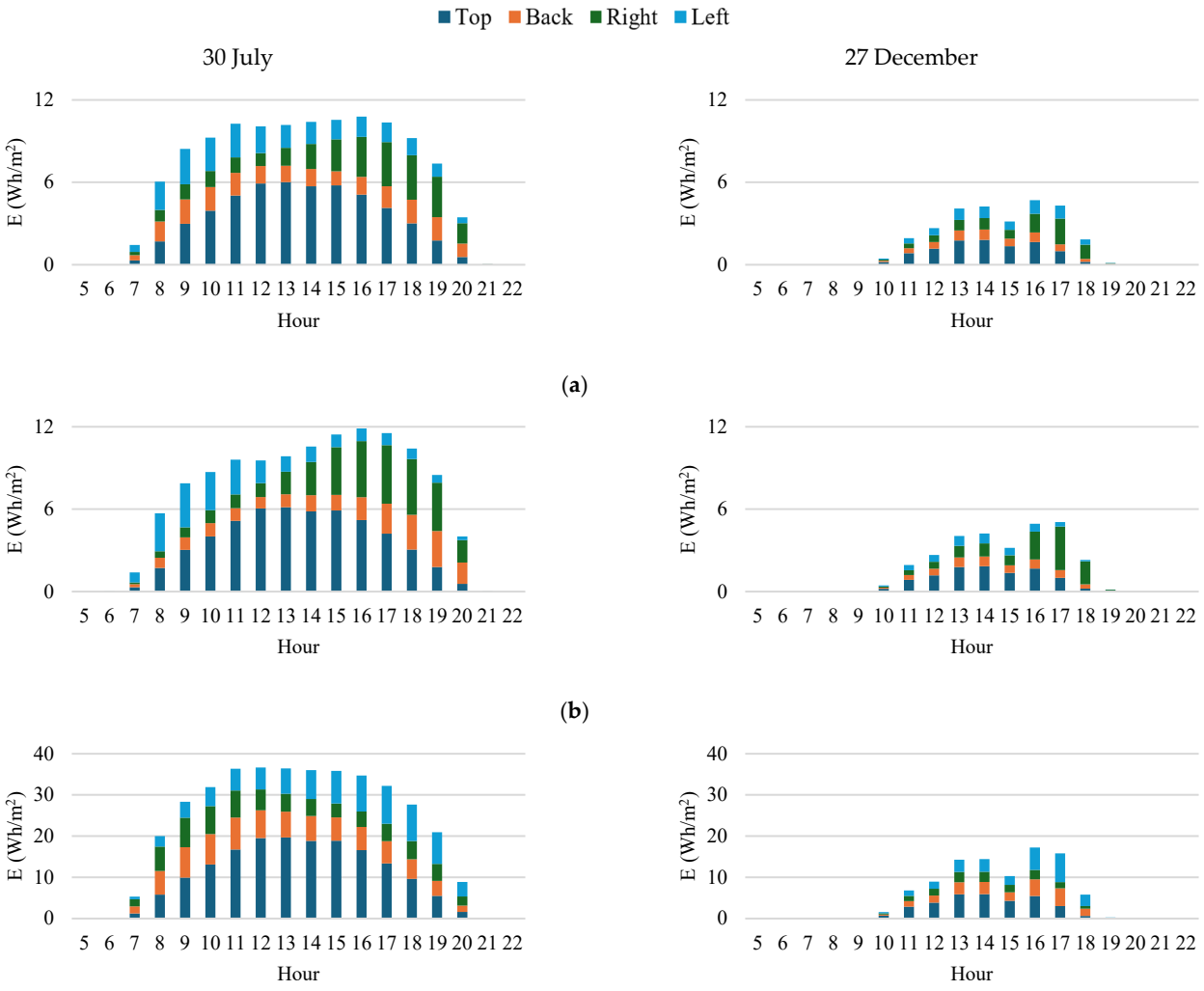

Figure 11. Energy production per square meter of PV installed on vehicle surfaces (roof, back, left, right) during three trips in Istanbul, conducted on 30 July and 27 December: (**a**) Trip 1, (**b**) Trip 2, (**c**) Trip 3.

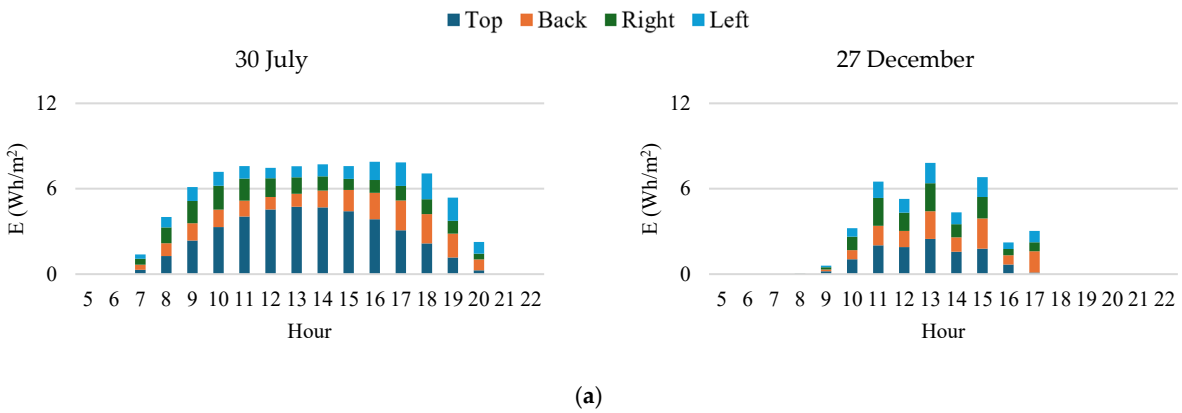

Figure 12. *Cont.*

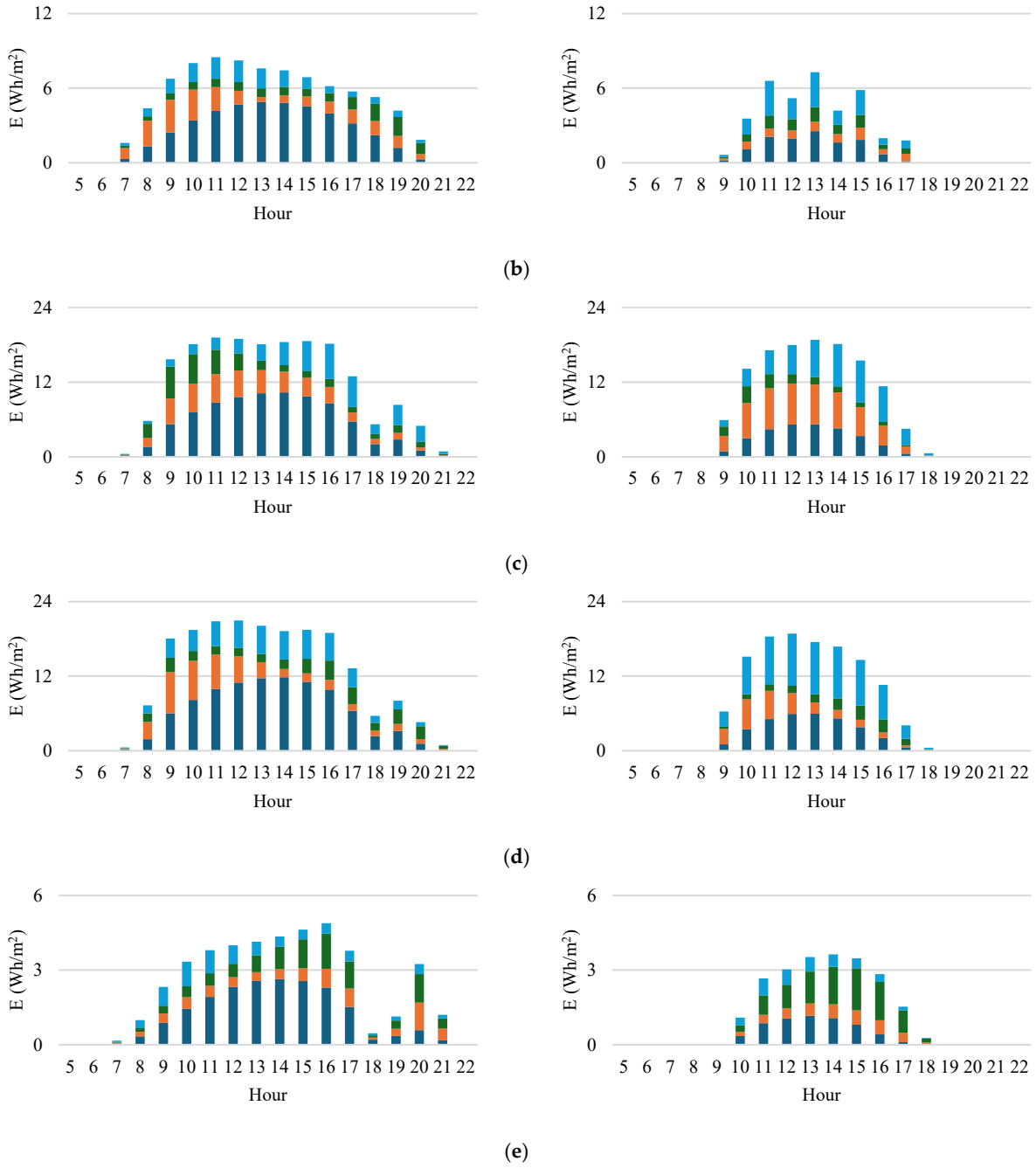

Figure 12. Energy production per square meter of PV installed on vehicle surfaces during trips in: (**a**) Palermo Trip 1, (**b**) Palermo Trip 2, (**c**) Rome Trip 1, (**d**) Rome Trip 2, (**e**) Milan.

5. Conclusions

This work uses a structured novel framework for evaluating the performance of vehicle-integrated photovoltaics in airport ground vehicles. The novelty lies in two aspects: first, the organization of modelling approaches into two complementary scenarios that address both limited-data and detailed-data conditions; second, the application of this framework to the underexplored but highly relevant context of ground operations in airports.

Scenario 1 provided a generalized methodology capable of producing long-term estimates of energy yield, avoided emissions, and grid parity using minimal input data. The results showed that even under conservative assumptions, VIPV can meaningfully extend the driving range of airport vehicles and contribute to decarbonization, with outcomes

strongly influenced by local irradiance, electricity prices, and grid carbon intensity. Scenario 2 illustrated the value of detailed driving data, highlighting how trip geometry, vehicle orientation, and seasonal or diurnal variations affect instantaneous energy production. As a further consideration, the analysis revealed that idle periods represent opportunities to maximize solar harvesting and improve system utility.

From a practical perspective, the proposed framework can serve as a decision-support tool for airport operators, fleet managers, and vehicle manufacturers to assess the technical and environmental feasibility of VIPVs' adoption. It enables the identification of optimal vehicle types, operating conditions, and parking strategies for maximizing solar utilization. Moreover, the model can support airport decarbonization planning, investment analysis, and sustainability reporting by quantifying avoided emissions and comparing on-vehicle solar generation with grid-based charging. By integrating the results of both generalized and data-driven approaches, the framework offers a scalable methodology that can be used for feasibility screening, operational planning, and policy evaluation.

Together, the two scenarios show the flexibility of the proposed framework. It can be applied as a simple screening tool in early-stage assessments and as a detailed model when comprehensive datasets are available. Beyond airports, the framework is transferable to other transport applications where VIPV may be relevant.

For future developments, the proposed framework could be coupled with airport digital twin platforms to enable dynamic optimization of fleet scheduling, energy management, and charging coordination. Integrating artificial intelligence (AI) and machine learning (ML) techniques, supported by larger and more detailed datasets, could further enhance model accuracy and enable adaptive control of vehicle charging, parking, and routing strategies to maximize solar energy utilization. In addition, future studies should investigate the techno-economic advantages of hybrid configurations that combine VIPV with stationary PV systems and energy storage, ultimately paving the way toward fully solar-powered and data-driven airport ground mobility ecosystems.

Author Contributions: Conceptualization, H.S., G.A. and M.C.B.; methodology, H.S., G.A. and M.C.B.; software, H.S. and G.M.; formal analysis, H.S., G.A. and F.V.; investigation, H.S.; resources, G.A.; data curation, H.S.; writing—original draft preparation, H.S., G.A. and M.C.B.; writing—review and editing, H.S., G.A., M.C.B. and P.R.; supervision: G.M., P.R. and F.V.; project administration, G.A. and M.C.B.; funding acquisition, G.A.; All authors have read and agreed to the published version of the manuscript.

Funding: This research received no external funding.

Institutional Review Board Statement: Not applicable.

Informed Consent Statement: Not applicable.

Data Availability Statement: Data are contained within the article.

Acknowledgments: The PhD work of Hamid Samadi contributing to this research is supported by the Italian National PhD in Photovoltaics—Curriculum: Design and Integration. This work was also supported by the European Union—NextGenerationEU (National Sustainable Mobility Center CN00000023, Italian Ministry of University and Research Decree n. 1033—17 June 2022, Spoke 12).

Conflicts of Interest: The authors declare no conflicts of interest.

List of Symbols and Parameters

A_{PV}	Effective PV area (m^2)	P	Power output of the PV system (W)
A_{Sur}	Available geometric surface area of the vehicle (m^2)	PR	Performance ratio
C_{life}	Total life cycle cost (€)	PV_{OUT}	Specific photovoltaic power output (kWh/kW_P per Year)
CF	Curvature factor	R	Driving-to-standby ratio
CI	Carbon intensity of the regional grid ($kgCO_2/kWh$)	T	PV module temperature (°C)
DHI	Diffuse horizontal irradiance (W/m^2)	T_a	Air temperature (°C)
DNI	Direct normal irradiance (W/m^2)	T_{ref}	Reference temperature (°C)
E	Energy generation (kWh)	U_0	Constant heat transfer component ($W/m^2°C$)
E_{life}	Total lifetime energy production (kWh)	U_1	Convective heat transfer component ($W/m^3s°C$)
F_1	Circumsolar component	WS	Wind speed (m/s)
F_2	Horizon brightness factor		Greek Symbols
G	Incident solar irradiance (W/m^2)	α	PV coverage ratio
G_b	Direct (beam) irradiance (W/m^2)	β	Surface tilt angle (°)
G_d	Diffuse irradiance (W/m^2)	η	Overall system efficiency
G_r	Reflected irradiance (W/m^2)	η_{Conv}	Power converter efficiency
GTI_{opta}	Global tilted irradiance at the optimum angle (kWh/m^2per Year)	η_{PV}	PV module efficiency
H_{STC}	Standard test condition irradiance (W/m^2)	$\eta_{Shading}$	Shading efficiency
h_{Roof}	Height of the vehicle roof (m)	θ_Z	Solar zenith angle (°)
k	Temperature coefficient (%/°C)	γ	Surface azimuth angle (°)
L	Standby charging losses (W)	γ_S	Solar azimuth angle (°)
$LCOE$	Levelized Cost of Electricity (€/kWh)		

References

1. Parhamfar, M. Towards green airports: Factors influencing greenhouse gas emissions and sustainability through renewable energy. *Next Res.* **2024**, *1*, 100060. [CrossRef]
2. Sreenath, S.; Sudhakar, K.; Yusop, A.F. Airport-based photovoltaic applications. *Prog. Photovolt. Res. Appl.* **2020**, *28*, 833–853. [CrossRef]
3. Ajayi, A.; Luk, P.C.-K.; Lao, L.; Khan, M.F. Energy Forecasting Model for Ground Movement Operation in Green Airport. *Energies* **2023**, *16*, 5008. [CrossRef]
4. Alruwaili, M.; Cipcigan, L. Airport electrified ground support equipment for providing ancillary services to the grid. *Electr. Power Syst. Res.* **2022**, *211*, 108242. [CrossRef]
5. Xiang, Y.; Cai, H.; Liu, J.; Zhang, X. Techno-economic design of energy systems for airport electrification: A hydrogen-solar-storage integrated microgrid solution. *Appl. Energy* **2021**, *283*, 116374. [CrossRef]
6. Samadi, H.; Ala, G.; Brano, V.L.; Romano, P.; Viola, F. Investigation of Effective Factors on Vehicles Integrated Photovoltaic (VIPV) Performance: A Review. *World Electr. Veh. J.* **2023**, *14*, 154. [CrossRef]
7. Samadi, H.; Ala, G.; Brano, V.L.; Romano, P.; Viola, F.; Miceli, R. Potential and Methods of Integrating Solar Cells into Vehicles. In Proceedings of the 2023 International Conference on Clean Electrical Power (ICCEP), Terrasini, Italy, 27–29 June 2023; pp. 715–720.
8. Yadav, B.K.; Yadav, R.; Jahangiri, M.; Priya, S.S.; Bajracharya, T.R.; Sudhakar, K. Decarbonizing airport using solar and wind farm: A case of Biratnagar, Nepal. *e-Prime* **2024**, *8*, 100583. [CrossRef]
9. Ollas, P.; Sigarchian, S.G.; Alfredsson, H.; Leijon, J.; Döhler, J.S.; Aalhuizen, C.; Thiringer, T.; Thomas, K. Evaluating the role of solar photovoltaic and battery storage in supporting electric aviation and vehicle infrastructure at Visby Airport. *Appl. Energy* **2023**, *352*, 121946. [CrossRef]
10. Araki, K.; Ota, Y.; Nishioka, K. Testing and rating of vehicle-integrated photovoltaics: Scientific background. *Sol. Energy Mater. Sol. Cells* **2024**, *280*, 113241. [CrossRef]
11. Peibst, R.; Fischer, H.; Brunner, M.; Schiessl, A.; Wöhe, S.; Wecker, R.; Haase, F.; Schulte-Huxel, H.; Blankemeyer, S.; Köntges, M.; et al. Demonstration of Feeding Vehicle-Integrated Photovoltaic-Converted Energy into the High-Voltage On-Board Network of Practical Light Commercial Vehicles for Range Extension. *Sol. RRL* **2021**, *6*. [CrossRef]

12. Pochont, N.R.; Sekhar, Y.R.; Brito, M.C.; Rao, V.T. Assessing the scope of vehicle integrated photovoltaics in urban driving conditions—Case study of a Tier-II city in southern India. *Sustain. Energy Technol. Assess.* **2024**, *72*, 104040. [CrossRef]
13. Wetzel, G.; Salomon, L.; Krügener, J.; Bredemeier, D.; Peibst, R. High time resolution measurement of solar irradiance onto driving car body for vehicle integrated photovoltaics. *Prog. Photovolt. Res. Appl.* **2021**, *30*, 543–551. [CrossRef]
14. Araki, K.; Ota, Y.; Nagaoka, A.; Nishioka, K. 3D Solar Irradiance Model for Non-Uniform Shading Environments Using Shading (Aperture) Matrix Enhanced by Local Coordinate System. *Energies* **2023**, *16*, 4414. [CrossRef]
15. Kutter, C.; Alanis, L.E.; Neuhaus, D.H.; Heinrich, M. Yield Potential of Vehicle Integrated Photovoltaics on Commercial Trucks and Vans 2021. Available online: https://www.researchgate.net/publication/355126708 (accessed on 20 July 2025).
16. Samadi, H.; Ala, G.; Imburgia, A.; Licciardi, S.; Romano, P.; Viola, F. Evaluating the Role of Vehicle-Integrated Photovoltaic (VIPV) Systems in a Disaster Context. *World Electr. Veh. J.* **2025**, *16*, 190. [CrossRef]
17. Oh, M.; Kim, S.-M.; Park, H.-D. Estimation of photovoltaic potential of solar bus in an urban area: Case study in Gwanak, Seoul, Korea. *Renew. Energy* **2020**, *160*, 1335–1348. [CrossRef]
18. Kim, H.; Ku, J.; Kim, S.-M.; Park, H.-D. A new GIS-based algorithm to estimate photovoltaic potential of solar train: Case study in Gyeongbu line, Korea. *Renew. Energy* **2022**, *190*, 713–729. [CrossRef]
19. Abdelhamid, M.; Pilla, S.; Singh, R.; Haque, I.; Filipi, Z. A comprehensive optimized model for on-board solar photovoltaic system for plug-in electric vehicles: Energy and economic impacts. *Int. J. Energy Res.* **2016**, *40*, 1489–1508. [CrossRef]
20. Mallon, K.R.; Assadian, F.; Fu, B. Analysis of On-Board Photovoltaics for a Battery Electric Bus and Their Impact on Battery Lifespan. *Energies* **2017**, *10*, 943. [CrossRef]
21. Faiman, D. Assessing the outdoor operating temperature of photovoltaic modules. *Prog. Photovolt. Res. Appl.* **2008**, *16*, 307–315. [CrossRef]
22. Duffie, J.A.; Beckman, W.A. *Solar Engineering of Thermal Processes*; Wiley and Sons: Hoboken, NJ, USA, 2013. [CrossRef]
23. Ota, Y.; Araki, K.; Nagaoka, A.; Nishioka, K. Facilitating vehicle-integrated photovoltaics by considering the radius of curvature of the roof surface for solar cell coverage. *Clean. Eng. Technol.* **2022**, *7*, 100446. [CrossRef]
24. Global Solar Atlas. Available online: https://globalsolaratlas.info/map (accessed on 6 April 2025).
25. Thiel, C.; Amillo, A.G.; Tansini, A.; Tsakalidis, A.; Fontaras, G.; Dunlop, E.; Taylor, N.; Jäger-Waldau, A.; Araki, K.; Nishioka, K.; et al. Impact of climatic conditions on prospects for integrated photovoltaics in electric vehicles. *Renew. Sustain. Energy Rev.* **2022**, *158*, 112109. [CrossRef]
26. Perez, R.; Ineichen, P.; Seals, R.; Michalsky, J.; Stewart, R. Modeling daylight availability and irradiance components from direct and global irradiance. *Sol. Energy* **1990**, *44*, 271–289. [CrossRef]
27. King, D.; Kratochvil, J.; Boyson, W. Measuring solar spectral and angle-of-incidence effects on photovoltaic modules and solar irradiance sensors. In Proceedings of the Conference Record of the Twenty Sixth IEEE Photovoltaic Specialists Conference — 1997, Anaheim, CA, USA, 29 September–3 October 1997.
28. VIPVLIB. Available online: https://github.com/hamidsmd/VIPVLIB (accessed on 5 July 2025).
29. Anderson, K.S.; Hansen, C.W.; Holmgren, W.F.; Jensen, A.R.; Mikofski, M.A.; Driesse, A. pvlib python: 2023 project update. *J. Open Source Softw.* **2023**, *8*, 5994. [CrossRef]
30. Vartiainen, E.; Masson, G.; Breyer, C.; Moser, D.; Román Medina, E. Impact of weighted average cost of capital, capital expenditure, and other parameters on future utility-scale PV levelised cost of electricity. *Prog. Photovolt. Res. Appl.* **2020**, *28*, 439–453. [CrossRef]
31. Electricity Maps. Available online: https://www.electricitymaps.com (accessed on 9 July 2025).
32. Electricity Prices for Non-household Consumers (2024-S2). Available online: https://ec.europa.eu/eurostat/databrowser/view/nrg_pc_205__custom_17400202/default/table?lang=en (accessed on 6 June 2025).
33. Electricity Prices. Available online: https://www.globalpetrolprices.com/electricity_prices/ (accessed on 13 July 2025).
34. US Dollar (USD). Available online: https://www.ecb.europa.eu/stats/policy_and_exchange_rates/euro_reference_exchange_rates/html/eurofxref-graph-usd.en.html (accessed on 13 July 2025).
35. Kumar, N.M.; Chopra, S.S.; Malvoni, M.; Elavarasan, R.M.; Das, N. Solar Cell Technology Selection for a PV Leaf Based on Energy and Sustainability Indicators—A Case of a Multilayered Solar Photovoltaic Tree. *Energies* **2020**, *13*, 6439. [CrossRef]
36. B. manufacturer Karsan, ELECTRIC MINIBUS with Zero Emissions, Karsan e-JEST. Available online: https://www.karsan.com/en/e-jest-highlights#e-jest-specs (accessed on 16 September 2024).
37. Alke' Airport Luggage Vehicles. Available online: https://www.alke.com/airport-luggage-vehicles (accessed on 5 May 2025).
38. Tous, L.; Govaert, J.; Harrison, S.; Carrière, C.; Barth, V.; Giglia, V.; Buchholz, F.; Chen, N.; Halm, A.; Faes, A.; et al. Overview of key results achieved in H2020 HighLite project helping to raise the EU PV industries' competitiveness. *Prog. Photovoltaics: Res. Appl.* **2023**, *31*, 1409–1427. [CrossRef]

Disclaimer/Publisher's Note: The statements, opinions and data contained in all publications are solely those of the individual author(s) and contributor(s) and not of MDPI and/or the editor(s). MDPI and/or the editor(s) disclaim responsibility for any injury to people or property resulting from any ideas, methods, instructions or products referred to in the content.